Electronic Supplementary Material (ESI) for Nanoscale.

Supporting Information for:

Alloying and Dealloying of $Au_{18}Cu_{32}$ Nanocluster at Precise Locations via Controlling the Electronegativity of Substituent Groups on Thiol Ligands

Li Tang,[a,‡] Bin Wang,[a,‡] Ru Wang[a] and Shuxin Wang*[a]

[a]*College of Materials Science and Engineering, Qingdao University of Science and Technology, Qingdao 266042, P. R. China.*

*E-mail of corresponding author: shuxin_wang@qust.edu.cn

This Supporting Information includes:
Figures S1-S10.
Tables S1-S3.

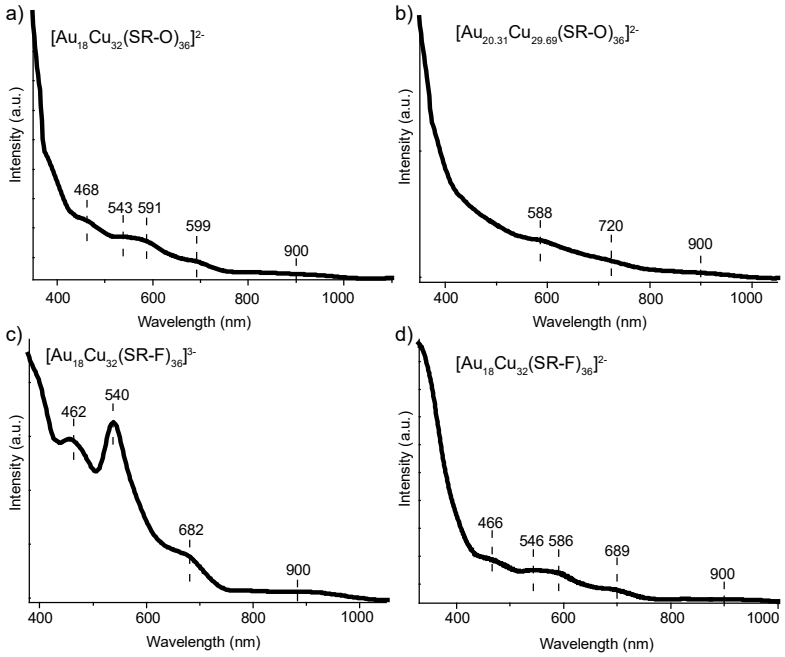

Fig. S1. UV-vis spectrum of a) **$[Au_{18}Cu_{32}(SR\text{-}O)_{36}]^{2-}$**, b) **$[Au_{20.31}Cu_{29.69}(SR\text{-}O)_{36}]^{2-}$**, c) **$[Au_{18}Cu_{32}(SR\text{-}F)_{36}]^{3-}$**, d) **$[Au_{18}Cu_{32}(SR\text{-}F)_{36}]^{2-}$**.

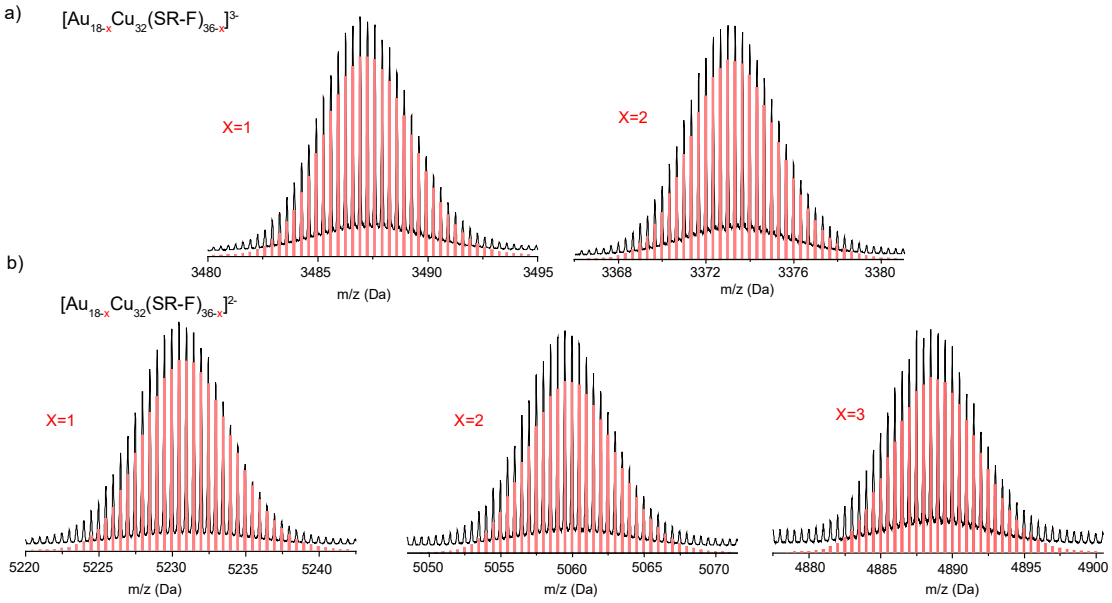

Fig. S2. Experimental mass spectrum matched with the theoretical simulation mass spectrum of a) **$[Au_{18}Cu_{32}(SR\text{-}F)_{36}]^{3-}$**, b) **$[Au_{18}Cu_{32}(SR\text{-}F)_{36}]^{2-}$**.

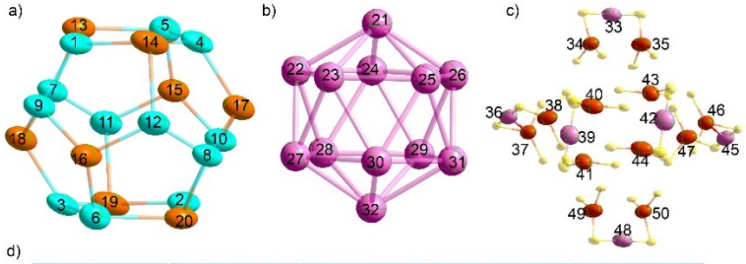

d)

site	Cu (%)	Au (%)	Total Cu	Total Au
1-2	0.807	0.193	1.614	0.386
3-4	0.801	0.199	1.602	0.398
5-6	0.826	0.174	1.652	0.348
7-8	0.774	0.226	1.548	0.452
9-10	0.850	0.150	1.70	0.30
11-12	0.786	0.214	1.572	0.428
13-20	100	0	8	0
21-32	0	100	0	12
33-50	100	100	12	6
Total Metal atoms			29.69	20.31
Composition from the crystal structure			$[Au_{20.31}Cu_{29.69}(SR\text{-}O)_{36}]^{2-}$	

Fig. S3. a), b), c) The occupancy information of metal sites 1-50 in **$[Au_{20.31}Cu_{29.69}(SR\text{-}O)_{36}]^{2-}$** nanoclusters. The molecular structure of both nanoclusters with thermal ellipsoids set at the 50% probability level. Color labels: rose/= Au, orange = Cu, turquoise= Au/Cu, S= yelow. For clarity, the C, H are not shown.

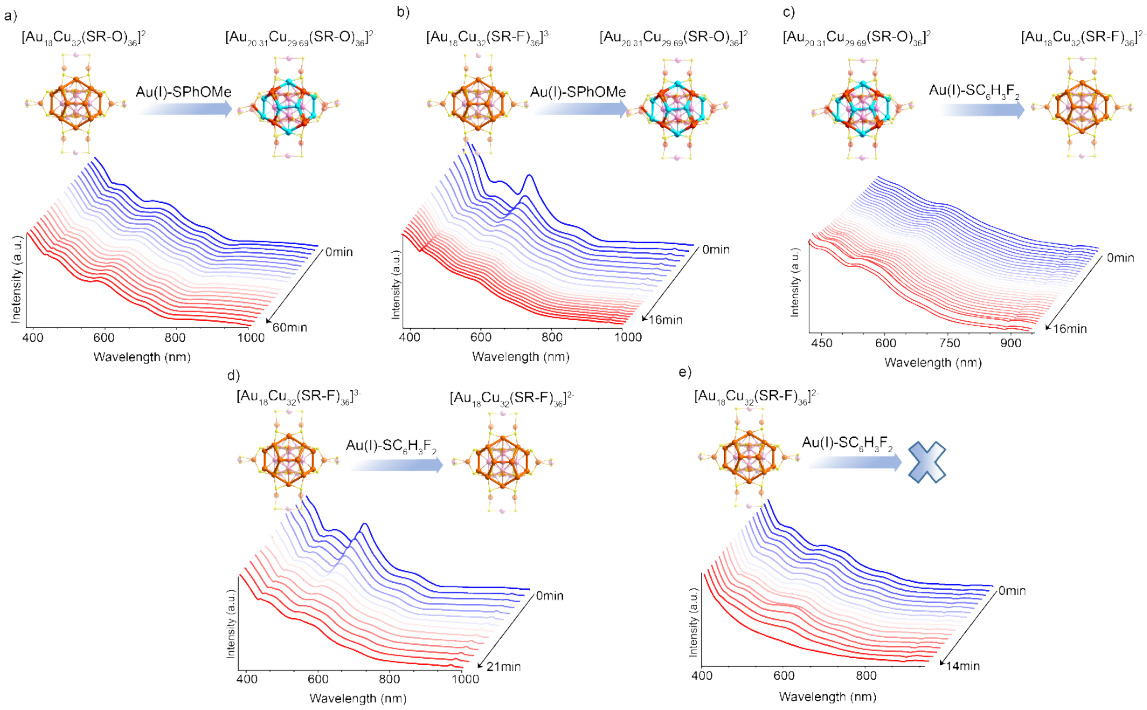

Fig. S4. Time-dependent UV-vis spectra of a) **$[Au_{18}Cu_{32}(SR\text{-}O)_{36}]^{2-}$** in CH_2Cl_2 after adding Au(I)-SPhOMe complex; b) **$[Au_{18}Cu_{32}(SR\text{-}F)_{36}]^{3-}$** in CH_2Cl_2 after adding Au(I)-SPhOMe complex; c) **$[Au_{18}Cu_{32}(SR\text{-}O)_{36}]^{2-}$** in CH_2Cl_2 after adding $HSC_6H_3F_2$ ligand. d) **$[Au_{18}Cu_{32}(SR\text{-}F)_{36}]^{3-}$** in CH_2Cl_2 after adding Au(I)-$SC_6H_3F_2$ complex; e) **$[Au_{18}Cu_{32}(SR\text{-}F)_{36}]^{2-}$** in CH_2Cl_2 after adding Au(I)-$SC_6H_3F_2$ complex.

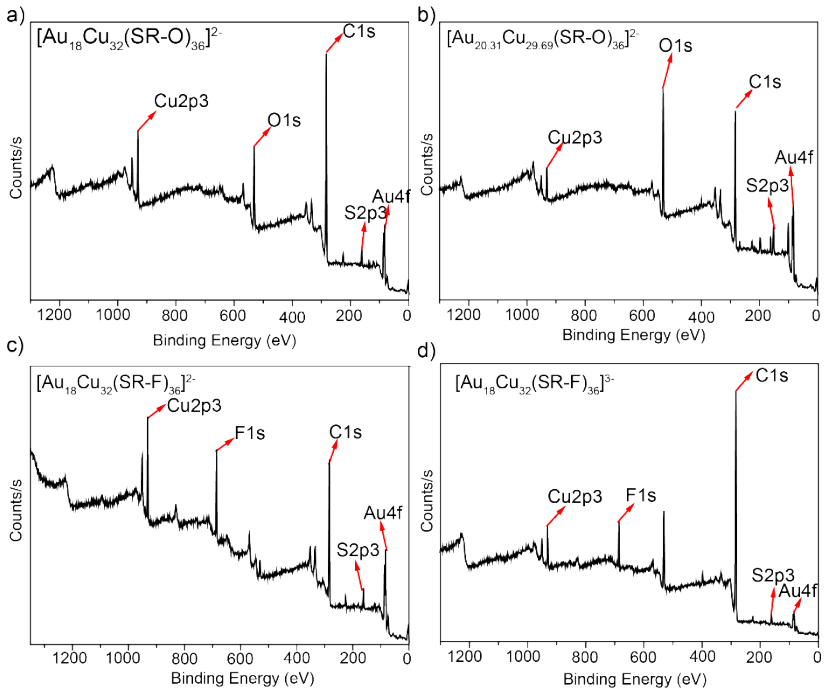

Fig. S5. XPS spectrum of a) **$[Au_{18}Cu_{32}(SR\text{-}O)_{36}]^{2-}$**, b) **$[Au_{20.31}Cu_{29.69}(SR\text{-}O)_{36}]^{2-}$**, c) **$[Au_{18}Cu_{32}(SR\text{-}F)_{36}]^{2-}$**, d) **$[Au_{18}Cu_{32}(SR\text{-}F)_{36}]^{3-}$**.

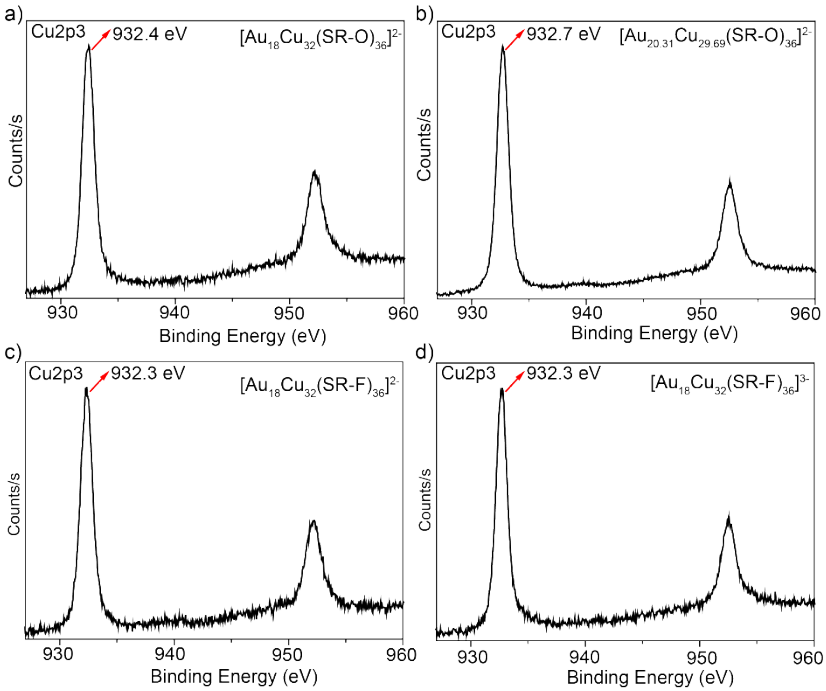

Fig. S6. X-ray photoelectron spectroscopy: Cu2p3 spectral region of a) **$[Au_{18}Cu_{32}(SR\text{-}O)_{36}]^{2-}$**, b) **$[Au_{20.31}Cu_{29.69}(SR\text{-}O)_{36}]^{2-}$**, c) **$[Au_{18}Cu_{32}(SR\text{-}F)_{36}]^{2-}$**, d) **$[Au_{18}Cu_{32}(SR\text{-}F)_{36}]^{3-}$**.

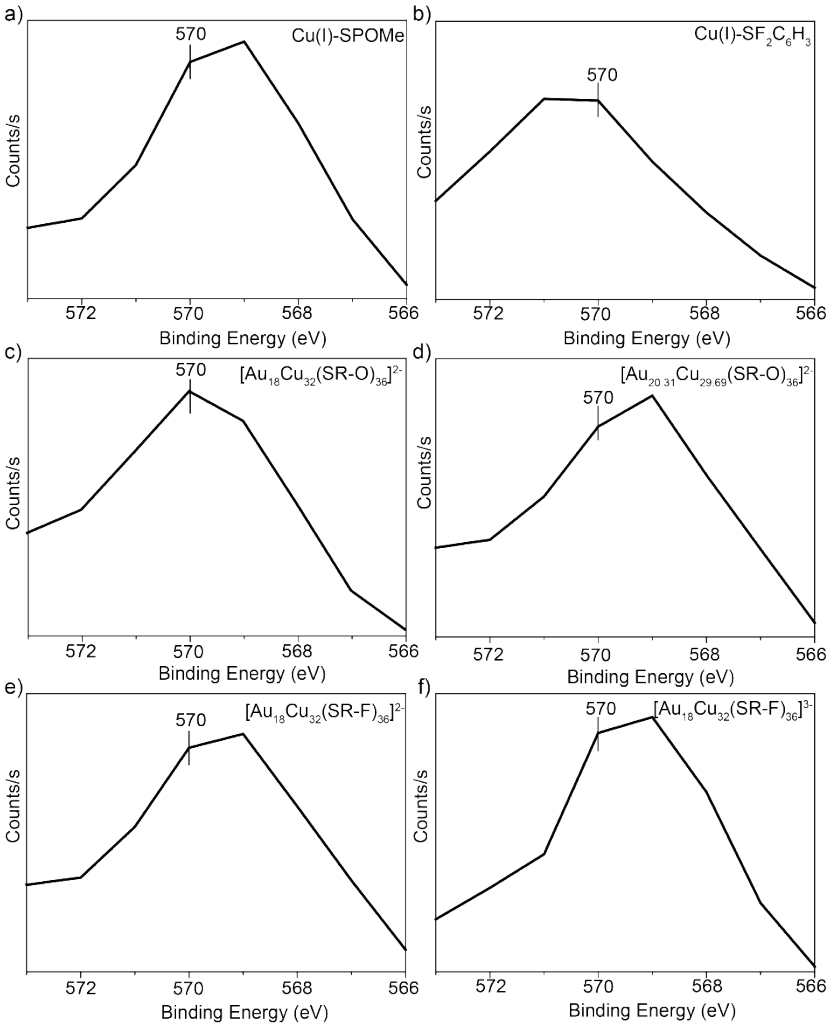

Fig. S7. Cu LMM XPS spectrum of a) Cu(I)-SPhOMe, b) Cu(I)-$SF_2C_6H_3$, c) **$[Au_{18}Cu_{32}(SR\text{-}O)_{36}]^{2-}$**, d) **$[Au_{20.31}Cu_{29.69}(SR\text{-}O)_{36}]^{2-}$**, e) **$[Au_{18}Cu_{32}(SR\text{-}F)_{36}]^{2-}$**, f) **$[Au_{18}Cu_{32}(SR\text{-}F)_{36}]^{3-}$**.

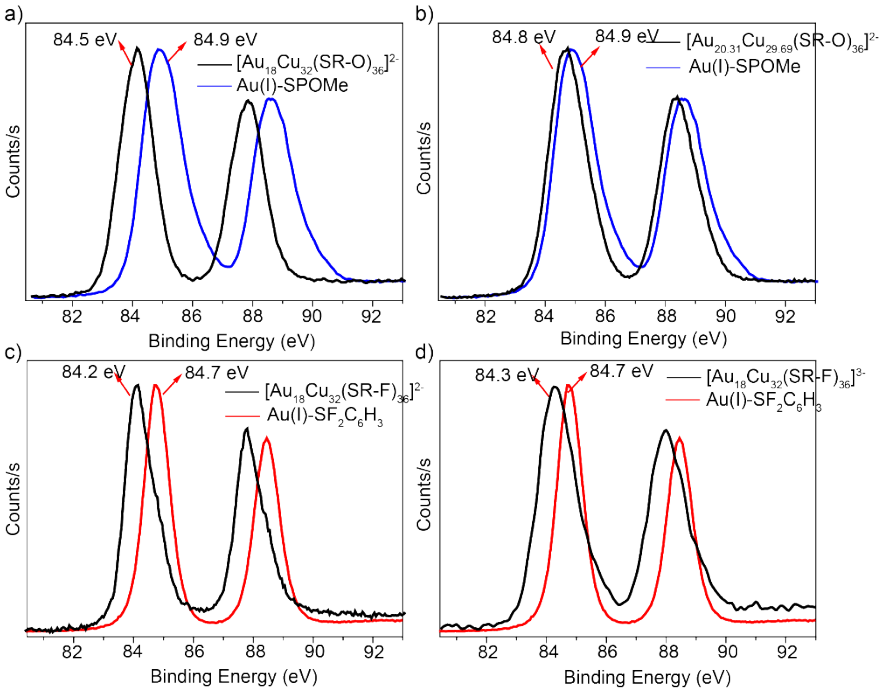

Fig. S8. X-ray photoelectron spectroscopy: Au4f spectral region of a) **$[Au_{18}Cu_{32}(SR\text{-}O)_{36}]^{2-}$**, b) **$[Au_{20.31}Cu_{29.69}(SR\text{-}O)_{36}]^{2-}$**, c) **$[Au_{18}Cu_{32}(SR\text{-}F)_{36}]^{2-}$**, d) **$[Au_{18}Cu_{32}(SR\text{-}F)_{36}]^{3-}$**.

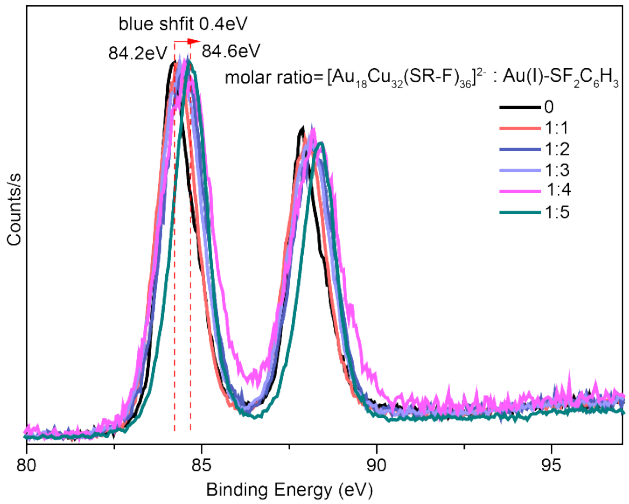

Fig. S9. X-ray photoelectron spectroscopy of **$[Au_{18}Cu_{32}(SR\text{-}F)_{36}]^{2-}$** adding various molar ratios of Au(SR-F) complex.

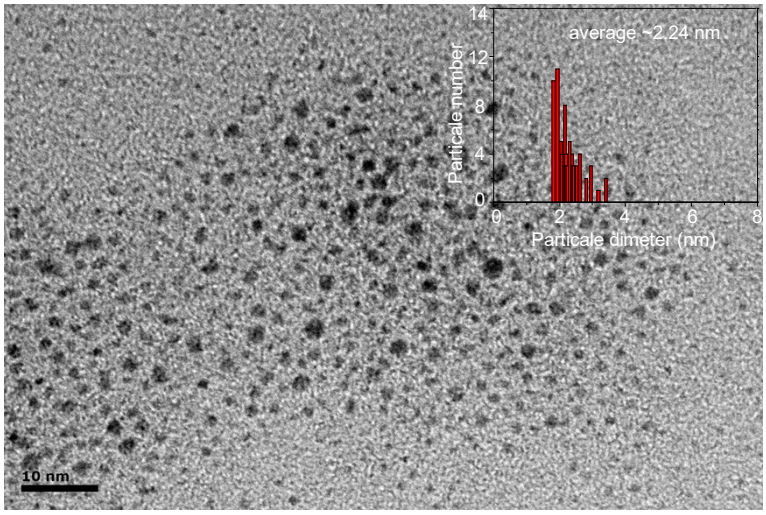

Fig. S10. TEM images of the products obtained by reaction of $[Au_{18}Cu_{32}(SR\text{-}F)_{36}]^{2-}$ with Au(SR-F) complex.

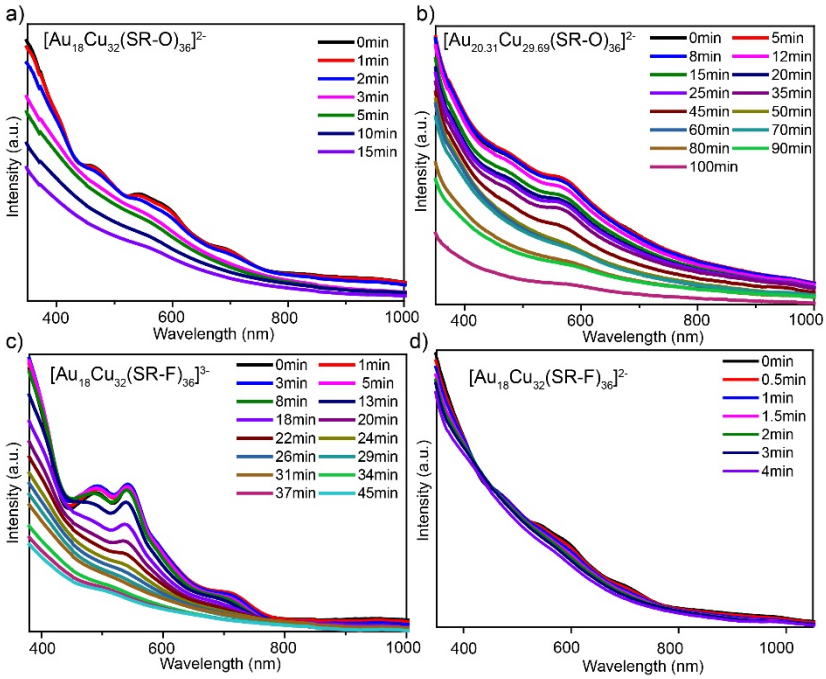

Fig. S11. UV-Vis spectra of DMF solutions of (a) $[Au_{18}Cu_{32}(SR\text{-}O)_{36}]^{2-}$, (b) $[Au_{20.31}Cu_{29.69}(SR\text{-}O)_{36}]^{2-}$, (c) $[Au_{18}Cu_{32}(SR\text{-}F)_{36}]^{3-}$, and (d) $[Au_{18}Cu_{32}(SR\text{-}F)_{36}]^{2-}$ heated in air at 50℃ for different times.

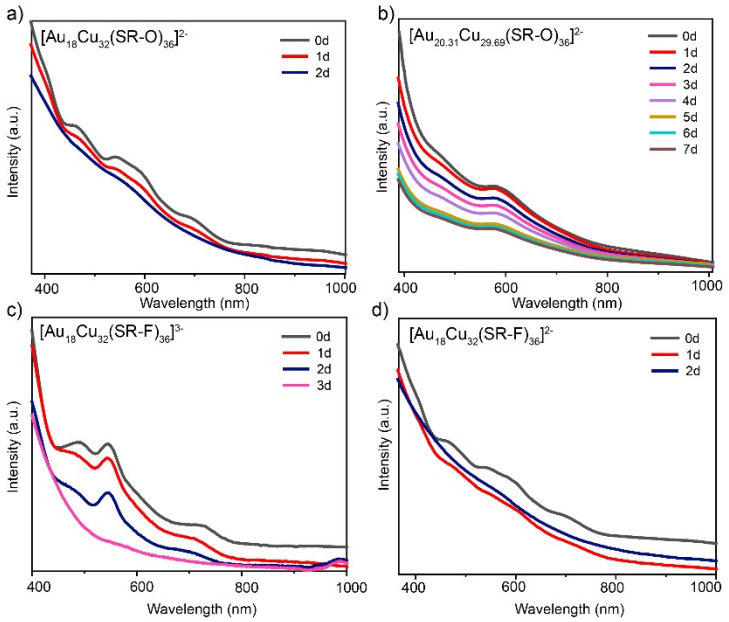

Fig. S12. UV-Vis spectra of DMF solutions of (a) $[Au_{18}Cu_{32}(SR\text{-}O)_{36}]^{2-}$, (b) $[Au_{20.31}Cu_{29.69}(SR\text{-}O)_{36}]^{2-}$, (c) $[Au_{18}Cu_{32}(SR\text{-}F)_{36}]^{3-}$, and (d) $[Au_{18}Cu_{32}(SR\text{-}F)_{36}]^{2-}$ at room temperature.

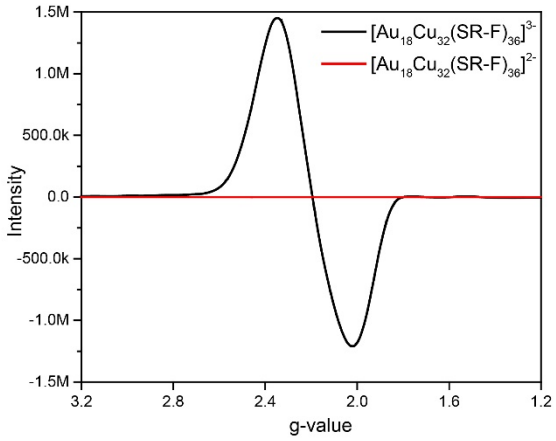

Fig. S13. EPR curves of $[Au_{18}Cu_{32}(SR\text{-}F)_{36}]^{3-}$(black) and $[Au_{18}Cu_{32}(SR\text{-}F)_{36}]^{2-}$(red).

Table S1. Crystal data and structure refinement for the **$[Au_{20.31}Cu_{29.69}(SR\text{-}O)_{36}]^{2-}$**.

Empirical formula	$C_{252}H_{252}Au_{20.31}Cu_{29.69}S_{36}O_{36}$	
CCDC	2026820	
Formula weight	10897.57	
Temperature/K	170	
Crystal system	triclinic	
Space group	P-1	
Unit cell dimensions	a = 21.3034(6) Å	α= 111.776(2) °
	b = 21.5883(7) Å	β= 118.542(2) °
	c = 21.9884(7)	γ= 96.201(2)°
Volume/Å^3	7728.8(4)	
Z	1	
Density (calculated)/Mg/m^3	2.341	
Absorption coefficient/mm^{-1}	22.433	
F(000)	5094.0	
Theta range for data collection/°	7.25 to 140.464	
Index ranges	-25<=h<=11, -26<=k<=24, -20<=l<=26	
Reflections collected	98463	
Independent reflections	28030 [Rint = 0.0686, Rsigma = 0.0636]	
Data / restraints / parameters	28030/2941/1474	
Goodness-of-fit on F^2	1.057	
Final R indices [I>2sigma(I)]	R1 = 0.0900, wR2 = 0.2464	
R indices (all data)	R1 = 0.1201, wR2 = 0.2691	
Largest diff. peak and hole/ e Å^{-3}	8.49/-2.37	

Table S2. Crystal data and structure refinement for the $[Au_{18}Cu_{32}(SR\text{-}F)_{36}]^{3-}$.

Identification code	$Au_{18}Cu_{32}(3,4\text{-}C_6H_3F_2S)_{30}$
CCDC	1960476
Formula weight	10653.57
Temperature/K	120.0
Crystal system	cubic
Space group	Fm-3c
Unit cell dimensions	a = 42.573(5) Å α= 90°
	b = 42.573(5) Å β= 90
	c = 42.573(5) Å γ= 90
Volume/Å^3	77161(28)
Z	8
Density (calculated)/Mg/m^3	1.834
Absorption coefficient/mm^{-1}	16.697
F(000)	39104.0
Theta range for data collection/°	12.3 to 139.43
Index ranges	-51<=h<=27, -51<=k<=44, -49<=l<=51
Reflections collected	124367
Independent reflections	3179 [R(int) = 0.0748, R_{sigma}=0.0173]
Data / restraints / parameters	3179/675/206
Goodness-of-fit on F^2	1.066
Final R indices [I>2sigma(I)]	R1 = 0.0554, wR2 = 0.1826
R indices (all data)	R1 = 0.0710, wR2 = 0.1976
Largest diff. peak and hole/ e Å^{-3}	1.29 and -1.50

Table S3. Comparison of different bond lengths in $[Au_{20.31}Cu_{29.69}(SR\text{-}O)_{36}]^{2-}$ and $[Au_{18}Cu_{32}(SR\text{-}F)_{36}]^{2-}$ crystal structures.

Bond type	$[Au_{20.31}Cu_{29.69}(SR\text{-}O)]^{2-}$		$[Au_{18}Cu_{32}(SR\text{-}F)_{36}]^{3-}$		Diff.
Bond length (Å)	range (Å)	average(Å)	range (Å)	average(Å)	(%)
Au-Au/within Au_{12} core	2.76-2.83	2.79	2.78-2.81	2.78	0.35
Au-M /(Au_{12}-M_{20} layer)	2.62-2.84	2.73	2.69-2.71	2.70	1.1
M-M/ (within the M_{20})	2.94-3.55	3.12	2.95-3.08	3.06	1.9
S-M/(within the ligand-M_{20})	2.22-2.40	2.30	2.22-2.37	2.31	0.43
Au-S/(within the ligand motif)	2.31-2.28	2.30	2.28-2.28	2.28	0.86
Cu-S/(within the ligand motif)	2.22-2.29	2.25	2.29-2.30	2.26	0.44